

## **Optical analysis of room temperature magnetron sputtered ITO films by reflectometry and spectroscopic ellipsometry**

**T. Lohner<sup>1\*</sup>, K. Jagadeesh Kumar<sup>2</sup>, P. Petrik<sup>1,3</sup>, A. Subrahmanyam<sup>2</sup>, I. Bársony<sup>1,3</sup>**

### **Affiliation:**

<sup>1</sup> Research Centre for Natural Sciences, Institute for Technical Physics and Materials Science, H-1121 Budapest, Konkoly Thege Miklós út 29-33, Hungary

<sup>2</sup> Semiconductor Laboratory, Department of Physics, Indian Institute of Technology Madras, Chennai 600036, India

<sup>3</sup> Department of Nanotechnology, University of Pannonia, H-8200 Veszprém, Hungary

### **Abstract**

Indium-tin-oxide (ITO) thin films were prepared by reactive magnetron sputtering, their optical constants and thickness were determined by spectral reflectometry (SR) in the wavelength range from 400 nm to 800 nm and spectroscopic ellipsometry (SE) in the wavelength range from 191 nm to 1690 nm. A comparative evaluation of the measured data from SR and SE has been made using the same single layer optical model based on the Cauchy dispersion relation. The introduction a surface roughness layer into the optical model considerably improved the fit quality during evaluation of SE data. Vertical inhomogeneity of the ITO thin films was assessed using a multilayer optical model describing porosity

gradient and the three-layer optical model suggested by Jung (Y.S. Jung, Thin Solid Films, **467**, 36 (2004)) from the SE data.

**Keywords:** film, optical, sputtering

## 1. Introduction

Thin films of tin doped indium oxide (ITO) have been subjected to intensive investigation by several workers, mainly because of the varied and versatile applications of these thin films.<sup>1-27</sup> These ITO thin films are quite complex and the properties are very sensitive to oxygen vacancies. The physical properties, in specific, the optical and electrical properties, of these thin films depend upon: (i) the thickness, (ii) the technique of preparation and (iii) on the growth parameters even in the same technique. With the advent of applications<sup>6,28-33</sup> demanding the preparation (manufacture) of these ITO films at relatively low temperature or preferably at room temperature (300 K) (mainly for the touch panel displays on plastics and top electrode for solar cells and electrochromic devices on flexible plastic substrates), our laboratory has reported the physical properties (including photocatalytic properties) of ITO thin films (as a function of thickness) prepared at room temperature (300 K) by reactive DC magnetron sputtering technique.<sup>27</sup>

The aim of the present communication is mainly (i) to report the optical constants of room temperature (300 K) magnetron sputtered ITO thin films and (ii) to compare the optical constants of these ITO thin films by spectral reflectometry (SR) (fast and cost effective) and

spectroscopic ellipsometry (SE) (time consuming, demand expertise for analyses). Characteristic optical properties of thin film structures can be derived from spectroscopic SE measurement, which is known to be a high-precision optical characterization technique.<sup>34-38</sup> Variable Angle Spectroscopic Ellipsometry (VASE) allows measurements at multiple angles of incidence. A new angle will change the length of the light penetrating through the materials. This can be advantageous in case of multilayers, as different path lengths usually deliver new information about the structure. Multiple angles are helpful to improve the confidence limits of the results yielded by the data evaluation. To the best of available knowledge with the authors, the optical constants of room temperature sputtered ITO are not reported in the literature.

Among the several reports on the optical constants of ITO thin films evaluated by spectroscopic ellipsometry,<sup>2-4,10,11,14,16,25,35</sup> the recent work by Jung<sup>14</sup> is most comprehensive. Jung investigated ITO thin films prepared under various DC magnetron sputtering conditions<sup>14</sup> using VASE. He analyzed the SE data using a model combining Drude and Lorentz oscillator terms. The three-layer optical model consists of a bottom layer just above the substrate (responsible for nucleation), the middle layer and the top layer with surface roughness. Although the technique and the growth parameters used in the present work are similar to those used by Jung, certain conditions are different: (i) in Jung's experiment the target was sintered ITO, in the present case the target was metallic, (ii) Jung applied DC sputtering technique, in the present case reactive DC sputtering was used, (iii) Jung selected single crystalline silicon for substrate, in the present experiment soda lime glass substrates were used, finally (iv) in Jung's experiment the thickness of the films was about 150 nm, in the present study the thickness values ranged from 165 to 1175 nm.

## 2. Experimental

All the details of the preparation of ITO thin films are given in reference.<sup>27</sup> Briefly, all the ITO thin films were deposited on cleaned soda lime glass substrates (2.5 cm x 2.5 cm) at room temperature (300 K) by reactive DC magnetron sputtering using a commercial sputtering system (ANELVA, model SPC-530H). The targets are metallic (In:Sn-90:10) with size: rectangular (38 cm x 13 cm). The target is powered to 0.2 W/cm<sup>2</sup> by a Magnetron power supply (M/s Advanced Energy Model: MDX-10kW). The flow rates of argon (sputter gas) and oxygen (reactive gas) were controlled through independent mass flow controllers (MKS model-1179A) keeping the ratio to 0.21 such that the chamber pressure is maintained at  $P_w = 3$  mbar. The average deposition rate is  $\sim 19$  nm/min. Before each deposition, the target was pre-sputtered with argon gas for 2 minutes in order to remove the surface oxide layer and to ensure the near virgin state of the target.

The ITO films are prepared with different thicknesses: they are labeled as S1-S6, S1 corresponding to a deposition time of 10 minutes (thickness  $t_{s1} = 165$  nm) and S6 ( $t_{s6} = 1175$  nm), corresponding to a deposition time of 60 minutes. The thickness (t), refractive index (n) and extinction coefficient (k) in the wavelength range 400 – 800 nm is measured by reflectometry (Filmetrics - F20).<sup>39</sup> Ellipsometric measurements have been done using a rotating compensator spectroscopic ellipsometer (Model M-2000DI produced by J.A. Woollam Co., Inc.) in the wavelength range of 191 -1690 nm with angles of incidence: of 55°, 60°, 65°, 70° and 75°; the measured data are analyzed using WVASE32 software.<sup>40</sup>

For the SE measurements, the rear face of the glass substrates was roughened to avoid disturbing reflection. The calculated spectra were fitted to the measured ones using a regression algorithm. The measure of the fit quality is the mean squared error (MSE). The unknown

parameters are allowed to vary until the minimum of MSE is reached. In order to avoid the “local” minimum<sup>22</sup> in the regression algorithm, a careful global search procedure has been applied in case of complex multilayer structures (involving a wide range of initial parameter values).

The optical constants of the substrates (soda lime glass) have been evaluated from SE measurements using a three-phase optical model consisting of the ambient (air), a surface roughness layer and the substrate. The roughness layer was taken into account on the basis of effective medium approximation,<sup>34,41</sup> the roughness layer consists of 50% of glass and 50% of void (a most valid assumption). The Cauchy dispersion relation was employed to describe the refractive index and the extinction coefficient of the glass. The five parameters of the Cauchy dispersion relation and the thickness of the roughness layer were considered as free variables.

The data analysis (191 – 1690 nm wavelength range) shows a surface roughness on the glass substrates to be  $3.8 \pm 0.5$  nm. The fitted values of the five parameters of the Cauchy dispersion relation were built in into the optical models of the ITO-glass structure.

### **3. Results and discussion**

For the sake of clarity, this section is divided into four parts:

First part describes the comparison between reflectometry and spectroscopic ellipsometry. Second part analyzes the spectroscopic ellipsometric data using four optical models and detailed analyses has been given including the depth profile. The third part analyzes the SE data following the optical model proposed by Jung. The fourth part of the work presents the optical analysis of sample S1 in the wavelength range 230-1690 nm.

### **A. Comparison of reflectometry and spectroscopic ellipsometry techniques:**

One of the objectives of our investigation is to evaluate the precision of thickness and refractive index obtained by reflectometry compared to those obtained from the Ellipsometric measurements: this objective is addressed in the first part of this section.

The refractive index (Fig.1) and extinction coefficient (Fig.2) data for the six samples obtained by reflectometry technique are reproduced for the sake of comparison.<sup>27</sup> Reflectometry gives the thickness and wavelength dependent refractive index and extinction coefficient of the thin film provided the base data on the refractive index of the substrate is fed to the program.<sup>39</sup> Reflectometry basically uses the well-known Cauchy dispersion relations:<sup>39</sup> this analysis is labeled as Model-1.

Model-1:

During the first evaluation of the measured SE data six free parameters were involved in the computation (Model-1): the thickness of the ITO layer and the other five are the parameters of the Cauchy dispersion relation. The thickness values obtained by evaluation of data measured by reflectometry together with thickness and MSE values obtained by evaluation of data measured by SE. Results are presented in Table 1. There is a considerable deviation between the measured and generated ellipsometric angles. The thicknesses and the MSE values are displayed in Table 1. The MSE values for the six samples from 97 to 227 are rather large; they indicate an inferior fit quality.

### **B. Analyses of SE data using four optical models (400-800 nm):**

The SE data are analyzed using four other optical models:

Model-2: surface roughness, Cauchy dispersion relation

Model-3: surface roughness, Drude + Lorentz

Model-4: surface roughness, Drude + Lorentz + porosity grading (400 – 800 nm)

Model-5: surface roughness, Drude + Lorentz + porosity grading (400- 1690nm)

All the results are given in Table 1 for clear comparison.

Model-2 to Model-5:

During the second evaluation (Model-2) of the measured SE data a two-layer optical model was chosen. In the optical model a surface roughness layer was considered on the top of the ITO film. The surface roughness layer means that the ITO material was mixed with 50% void on the basis of the effective medium approximation.<sup>34,41</sup> The only free parameter is the thickness of the surface roughness layer. Altogether seven free parameters were involved in the computation: two of them are thickness-related parameters (thickness of the surface roughness layer and the thickness of the ITO layer); the other five ones are the parameters of the Cauchy dispersion relation. In the case of two-layer (surface roughness layer plus ITO layer) or multilayer optical models (surface roughness layer plus ITO layer with porosity grading) the “Thickness” is the sum of the thickness of the ITO layer and half of the thickness of the surface roughness layer.

The evaluation yielded MSE values from 15 to 41 for the six samples as one can see in Table 1. These values show a considerable

decrease if we compare to the previous case (Model-1). This means that the agreement between the measured and computed spectra improved substantially. This reflects that ellipsometry is very sensitive to the top surface condition, i.e. the insertion of the surface roughness layer into the optical model.

During the third evaluation (Model-3) of the measured SE data eight free parameters were involved in the computation: two of them are thickness-related parameters (thickness of the surface roughness layer and the thickness of the ITO layer), the other six ones are in connection with the Lorentz oscillator and the Drude oscillator. Traditionally, the wavelength dependence of the complex refractive index of ITO material have been described by use of Lorentz and Drude oscillators.<sup>2,25</sup> The evaluation yielded MSE values from 14 to 23 for the six samples as one can see in Table 1. This means that the agreement between the measured and computed spectra is satisfactory. Fig. 3 shows the wavelength dependence of the refractive index for the six ITO films using Model-3. Fig. 4 shows the wavelength dependence of the extinction coefficient for the six ITO films.

In the fourth evaluation (Model-4) an additional free parameter was introduced in the computation: it describes the volume fraction of void. The optical model consists of the surface roughness layer and 99 sublayers. The void gradient was implemented through 99 sublayers; each sublayer can be considered as a mixture of ITO material and void (according to the Bruggeman effective medium approximation.<sup>34,41</sup> The ninth free parameter describes the void volume fraction of the first thin sublayer below the surface roughness layer. The void fraction of the last thin sublayer (this thin sublayer is adjacent to the glass substrate) is zero. In other words, the index grading in the ITO film was assumed to be linear with depth, and calculated by sub dividing the ITO layer into many thin slabs (laminae), each of constant refractive index. The void

fraction of the sublayer adjacent to the surface roughness layer and the refractive index of the sublayer adjacent to the glass substrate at wavelength of 474 nm is given for Model-4.

Fig. 5 and Fig. 6 shows the measured and generated values of the ellipsometric angles  $\Psi$  and  $\Delta$  for sample S4 for the case of the evaluation by Model-4. The agreement between the measured and the calculated (simulated) spectra reveals the quality of the fit. The void fraction of the sublayer adjacent to the surface roughness layer is given in Table 1 for the six samples. The introduction of the new free parameter (void volume fraction) led to the decrease in MSE for all the six samples in the evaluation compared to the MSE values obtained during the evaluation applying Model-3. The fifth evaluation was performed in the wavelength range of 400-1690 nm. The results are also shown in Table 1. The constant refractive index shown in Table 1 belongs to the sublayer adjacent to the glass substrate for Model-4 and Model-5.

Fig.7 depicts the refractive index and the extinction coefficient in function of the wavelength for the top and the bottom sublayers of the ITO film for sample S1. Fig. 8 shows the depth profile of the refractive index for the ITO film of sample S1. The refractive index at 474 nm of the sublayer adjacent to the glass substrate is given for all six samples in Table 1. These refractive index values ranging from 2.14 to 2.20 are close to the refractive index value of the bulk ITO (2.19) mentioned by Kim et al.<sup>20</sup>

### **C. Comparison with the model proposed by Jung:** <sup>14</sup>

The three-layer optical model constructed by Jung consists of a bottom layer just above the substrate (responsible for nucleation), a middle layer and the top layer representing the surface roughness.

Similar evaluations were performed on the SE data measured by us involving 15 free parameters. Since Jung performed the evaluations in the wavelength range of 300 – 1000 nm, we have chosen the same range. The free parameter describing the thickness of the bottom ITO layer was allowed to change between 0 nm and 100 nm in the global search procedure. From Table 2 one can see that the fit results are in the range of 20 – 53 nm for this parameter (depending on the total thickness). Jung published a value of 30 nm for the thickness of the bottom ITO layer (the total thickness of the films was about 150 nm in his experiment).<sup>14</sup> Fig. 9 displays the wavelength dependence of refractive index and extinction coefficient of the bottom layer obtained from evaluation of SE data measured on sample S1. Fig. 10 shows the refractive index and the extinction coefficient vs. wavelength for the top ITO layer for sample S1 using evaluation of SE data based on the Jung model. In addition we evaluated the SE data using a two-layer optical model with the combination of a Drude oscillator and a Lorentz oscillator and porosity grading also in the wavelength range of 300 – 1000 nm. It is remarkable that the MSE values are significantly lower for evaluations performed using the so called Jung model than in the case of the optical model constructed with a linear porosity grading.

ITO films usually grow with a graded microstructure which introduces grading or vertical inhomogeneity into the complex refractive index of the films<sup>3,4,14,42</sup>. Evaluation using a vertically homogeneous ITO layer in the optical model in the visible spectral range (from 400 nm to 800 nm) provides the approximate film thickness and refractive index (this model is what is being employed in Reflectometry measurements). To obtain more accurate values it is necessary to take into account the vertical inhomogeneity in the optical model. The Jung model implements the vertical inhomogeneity by using two sublayers for the bulk ITO film, each sublayer described by free parameters concerning the thickness and the quantities belonging to the dispersion relation. During the evaluation in the step of the global minimum search 15 free parameters should be

varied within the carefully prescribed limits in order to find the global minimum for MSE in the case of Jung model.

The Model-4 based on a void gradient implemented through 99 sublayers of equal thickness (linear porosity grading) for describing vertical inhomogeneity. Altogether 9 free parameters should be varied in order to find the global minimum for MSE. However, the computation time is considerable longer than in the case of the Jung model, because the treatment of the 100-layer structure (surface roughness layer + 99 sublayers) needs a lot of time.

In Model-4 and Model-5 the bulk ITO film was divided into 99 sublayers of equal thickness, so the thickness of the sublayer changes from sample to sample. The constant refractive index shown in Table 1 belongs to the sublayer adjacent to the glass substrate. The sublayer thicknesses calculated in Model-4 and Model-5 are given in Table 1A.

We have found that the MSE values are significantly lower for evaluations with Jung model than for evaluations performed with Model-4, with linear porosity grading.

#### **D. Evaluation of optical constants of ITO in the wavelength range 230 – 1690 nm:**

Results on sample S1 are presented here. The analyses being similar, the data for other samples (S2-S6) is not presented in this communication. Fig. 11 and Fig. 12 show the measured and generated psi and delta values for the wavelength range of 230 - 1690 nm, the significant deviation disappeared from the generated psi spectra at the vicinity of the starting wavelength. The MSE=20.52.

The Fig. 13 and Fig. 14 are displaying the refractive index and the extinction coefficient versus wavelength for the bottom and top ITO layer for

sample S1 using evaluation of SE data in the wavelength range of 230 – 1690 nm based on the model proposed by Jung.

#### **4. Conclusions**

The optical constants: refractive index ( $n$ ) and extinction coefficient ( $k$ ) for different thicknesses of ITO thin films measured by spectral reflectometry (400 – 800 nm) and spectroscopic ellipsometry (230 – 1600 nm) are presented in this communication. The ITO thin films have been prepared by reactive DC magnetron sputtering at room temperature (300 K) on soda lime glass substrates employing a metal alloy target which quite likely introduces (due to unstable process) a vertically inhomogeneous ITO layer. Results show that the optical constants measured by spectral reflectometry are comparable with those evaluated by SE. Detailed analyses of SE data have been executed using five optical models. To analyze the graded structure of the films, optical models describing porosity gradient were used. The sublayer thicknesses are calculated. Most significant improvement of the fit quality was obtained by introducing a surface roughness layer. The SE data are also analyzed using the optical model proposed by Jung who suggested for description of the bulk ITO film two independent layers. We have found that the MSE values are significantly lower for evaluations with Jung model than for evaluations performed with linear porosity grading.

From the present study, it may be inferred that accurate estimate of the thickness and refractive index may be obtained if one follows the strategy: (i) first one may apply the Cauchy dispersion relation in the visible spectral range (approximately from 400 nm to 800 nm) for the determination of the approximate film thickness and refractive index; (ii) in the second step one may use the three-layer optical model (surface roughness layer and two sublayers) elaborated by Jung to handle the vertical inhomogeneity; (iii) the approximate film thickness and refractive

index values determined in the first evaluation step may serve to establish reasonable parameter limits for the global search procedure in the second step.

### **Acknowledgements**

The authors acknowledge the support of the Hungarian-Indian R&D Cooperation Program under the contracts No.TÉT10-1-2011-0305 and INT/HUN/P-O4/2012 dated 27Sept2012 (DST, Govt of India project sanction:TET\_09\_IN\_DST\_KFI dated 21 March 2012), the support from the Hungarian Scientific Research Fund (OTKA No.K81842), and the Hungarian National Development Agency grant TÁMOP- 4.2.2/B-10/1-2010-0025; Department of Science and Technology, Government of India (INT/HUN/P-04/2012 dated 15 Dec 2009) for supporting the project.

### **References:**

1. J.P. Zheng and H.S. Kwok: Preparation of indium tin oxide films at room temperature by pulsed laser deposition. *Thin Solid Films* **232**, 99 (1993).
2. W. Fukarek and H. Kersten: Application of dynamic in situ ellipsometry to the deposition of tin-doped indium oxide films by reactive direct-current magnetron sputtering. *J. Vac. Sci. Technol. A* **12**, 523 (1994).

3. J.A. Woollam, W.A. McGahan, and B. Johs: Spectroscopic ellipsometry studies of indium tin oxide and other flat panel display multilayer materials. *Thin Solid Films* **241**, 44 (1994).
4. R.A. Synowicki: Spectroscopic ellipsometry characterization of indium tin oxide film microstructure and optical constants. *Thin Solid Films* **313/314**, 394 (1998).
5. E. Benamar, M. Rami, C. Messaoudi, D. Sayan and A. Ennaoui: Structural, optical and electrical properties of indium tin oxide thin films prepared by spray pyrolysis. *Sol. Energy Mater. Sol. Cells* **56**, 125 (1999).
6. J.A. Dobrowolski, L. Li and J.N. Hilfiker: Long-Wavelength Cutoff Filters of a New Type. *Appl. Opt.* **38**, 4891 (1999).
7. J. George and C.S. Mourn: Electrical and optical properties of electron beam evaporated ITO thin films. *Surf. Coat. Technol.* **132**, 45 (2000).
8. Y. Han, D. Kim, J.S. Cho, S.K. Koh and Y.S. Song: Tin-doped indium oxide (ITO) film deposition by ion beam sputtering. *Sol. Energy Mater. Sol. Cells.* **65**, 211 (2001).

9. M. Martino, A. Luches, M. Fernandez, P. Anobile and V. Petnizzelli: Characterization of thin indium tin oxide films deposited by pulsed XeCl laser ablation. *J. Phys. D: Appl. Phys.* **34**, 2606 (2001).
10. M. Losurdo, M. Giangregorio, P. Capezzuto, G. Bruno, R. DeRosa, F. Roca, C. Summonte, J. Plá, and R. Rizzoli: Parametrization of optical properties of indium–tin–oxide thin films by spectroscopic ellipsometry: Substrate interfacial reactivity. *J. Vac. Sci. Technol. A* **20**, 37 (2002).
11. H. El Rhaleb, E. Benamar, M. Rami, J.P. Roger, A. Hakam and A. Ennaoui: Spectroscopic ellipsometry studies of index profile of indium tin oxide films prepared by spray pyrolysis. *Appl. Surf. Sci.* **201**, 138 (2002).
12. T.C. Gorjanc, D. Lemig, C. Py and D. Roth: Room temperature deposition of ITO using r.f. magnetron sputtering. *Thin Solid Films* **413**, 181 (2002).
13. K. Maki, N. Komiya and A. Suzuki: Fabrication of thin films of ITO by aerosol CVD. *Thin Solid Films* **445**, 224 (2003).
14. Y.S. Jung: Spectroscopic ellipsometry studies on the optical constants of indium tin oxide films deposited under various sputtering conditions. *Thin Solid Films* **467**, 36 (2004).

15. M. Yamaguchi, A. Ide-Ektesabi, H. Nomura and N. Yasiu: Characteristics of indium tin oxide thin films prepared using electron beam evaporation. *Thin Solid Films* **447/448**, 115 (2004).
16. Y.S. Jung: A spectroscopic ellipsometry study on the variation of the optical constants of tin-doped indium oxide thin films during crystallization. *Solid State Commun.* **129**, 491 (2004).
17. F.F. Ngaffo, A.P. Caricato, A. Fazzi, M. Fernandez, S. Lattante, M. Martino and F. Romano: Deposition of ITO films on SiO<sub>2</sub> substrates. *Appl. Surf. Sci.* **248**, 428 (2005).
18. H.C. Lee and O.O. Park: The evolution of the structural, electrical and optical properties in indium-tin-oxide thin film on glass substrate by DC reactive magnetron sputtering. *Vacuum* **80**, 880 (2006).
19. A. Krasilnikova Sytchkova, M.L. Grilli, S. Boycheva and A. Piegari: Optical, electrical, structural and microstructural characteristics of r.f. sputtered ITO films developed for art protection coating. *Appl. Phys. A.* **89**, 63 (2007).

20. J.K. Kim, S. Chhajed, M.F. Schubert, E.F. Schubert, A.J. Fischer, M.H. Crawford, J. Cho, H. Kim and C. Sone: Light-Extraction Enhancement of GaInN Light-Emitting Diodes by Graded-Refractive-Index Indium Tin Oxide Anti-Reflection Contact. *Adv. Mater.* **20**, 801 (2008).
21. L. Hao, X. Diao, H. Xu, B. Gu and T. Wang: Thickness dependence of structural, electrical and optical properties of indium tin oxide (ITO) films deposited on PET substrates. *Appl. Surf. Sci.* **254**, 3504 (2008).
22. T.S. Sathiaraj: Effect of annealing on the structural, optical and electrical properties of ITO films by RF sputtering under low vacuum level. *Microelectron. J.* **39**, 1444 (2008).
23. A. Iljinas, I. Mockevicius, M. Andrulevicius, S. Meskinis and S. Tamulevicius: Growth of ITO thin films by magnetron sputtering: OES study, optical and electrical properties. *Vacuum* **83**, S118 (2009).
24. C. Tejo-Cruz, A. Mendoza-Galván, A. M. López-Beltrán, and M. Garcia-Jimenez: Effects of air annealing on the optical, electrical, and structural properties of indium-tin oxide thin films. *Thin Solid Films* **517**, 4615 (2009).

25. S. D'Elia, N. Scaramuzza, F. Ciuchi, C. Versace, G. Strangi and R. Bartolino: Ellipsometry investigation of the effects of annealing temperature on the optical properties of indium tin oxide thin films studied by Drude–Lorentz model. *Appl. Surf. Sci.* **255**, 7203 (2009).
26. V. Senthilkumar, P. Vickraman, M. Jayachandran and C. Sanjeeviraja: Structural and optical properties of indium tin oxide (ITO) thin films with different compositions prepared by electron beam evaporation. *Vacuum* **84**, 864 (2010).
27. K.J. Kumar, N.R.C. Raju and A. Subrahmanyam: Thickness dependent physical and photocatalytic properties of ITO thin films prepared by reactive DC magnetron sputtering. *Appl. Surf. Sci.* **257**, 3075 (2011).
28. H. Kim, A. Pique, J.S. Horowitz, H. Mattoussi, H. Murata, Z.H. Kafafi, and D.B. Chrisey: Indium tin oxide thin films for organic light-emitting devices. *Appl. Phys. Lett.* **74**, 3444 (1999).
29. V. Teixeira, H.N. Cui, L.J. Meng, E. Fortunato and R. Martins: Amorphous ITO thin films prepared by DC sputtering for electrochromic applications. *Thin Solid Films* **420**, 70 (2002).
30. J.B. Chu, S.M. Huang, H.B. Zhu, X.B. Xu, Z. Sun, Y.W. Chen and F.Q. Huang: Preparation of indium tin oxide thin films without external heating for application in solar cells. *J. Non-Cryst. Solids* **354**, 5480 (2008).

31. H.P. Lobl, M. Huppertz and D. Mergel: ITO films for antireflective and antistatic tube coatings prepared by d.c. magnetron sputtering. *Surf. Coat. Technol.* **82**, 90 (1996).
32. T. Sako, A. Ohmi, H. Yumoto and K. Nishiyama: ITO-film gas sensor for measuring photodecomposition of NO<sub>2</sub> gas. *Surf. Coat. Technol.* **142/144**, 781 (2001).
33. M. Balestrieri, D. Pysch, J.-P. Becker, M. Hermle, W. Warta and S.W. Glunz: Characterization and optimization of indium tin oxide films for hetero junction solar cells. *Sol. Energy Mater. Sol. Cells* **95**, 2390 (2011).
34. E.A. Irene: Applications of spectroscopic ellipsometry to microelectronics. *Thin Solid Films* **233**, 96 (1993).
35. T.F. Stoica, M. Gartner, M. Losurdo, V. Teodorescu, M. Blanchin, T. Stoica and M. Zaharescu: Spectroellipsometric study of the sol-gel nanocrystalline ITO multilayer films. *Thin Solid Films* **455/456** 509 (2004).
36. H. Fujiwara, *Spectroscopic Ellipsometry: Principles and Applications*. (John Wiley and Sons, Chichester, England, 2007).

37. C. Major, G. Juhász, Z. Horváth, O. Polgár, and M. Fried: Wide angle beam ellipsometry for extremely large samples. *physica status solidi c* – Current Topics in Solid State Physics **5**, (5) 1077 (2008).

38. M. Kulik, J. Zuk, A. Drozdiel, K. Pyszniak, F.F. Komarov and W. Rzedkiewicz: RBS-C and ellipsometric investigations of radiation damage in hot-implanted GaAs layers. *Mater. Sci. Eng. B* **176**, 340 (2011).

39. [www.filmetrics.com](http://www.filmetrics.com)

40. J.A. Woollam Co., Inc. ([www.jawoollam.com](http://www.jawoollam.com))

41. D.E. Aspnes: Optical properties of thin films. *Thin Solid Films* **89**, 249 (1982).

42. Kun-San Tseng, Yu-Lung Lo, *Optical Materials Express* **4**, 43 (2014).

### **Figure Captions:**

Fig. 1. Refractive index (n) variation of ITO thin films for different thicknesses (S1-S6) in the wavelength range of 400-800 nm

evaluated from reflectometry data.

Fig. 2. Extinction coefficient ( $k$ ) variation of ITO thin films for different thicknesses (S1-S6) in the wavelength range of 400-800 nm evaluated from reflectometry data.

Fig.3. Refractive index ( $n$ ) variation of ITO thin films for different thicknesses (S1-S6) in the wavelength range of 400-800 nm using a two-layer optical model with the combination of a Drude oscillator and a Lorentz oscillator for evaluation of SE data.

Fig. 4. Extinction coefficient ( $k$ ) variation of ITO thin films for different thicknesses (S1-S6) in the wavelength range of 400-800 nm using a two-layer optical model with the combination of a Drude oscillator and a Lorentz oscillator for evaluation of SE data.

Fig. 5. Measured and generated ellipsometric angle  $\Psi$  for sample S4 evaluated using a two-layer optical model with the combination of a Drude oscillator and a Lorentz oscillator using porosity grading.

Fig. 6. Measured and generated ellipsometric angle  $\Delta$  for sample S4 evaluated using a two-layer optical model with the combination of a

Drude oscillator and a Lorentz oscillator using porosity grading.

Fig.7. The refractive index and the extinction coefficient versus wavelength for the top and the bottom sublayer of the ITO film for sample S1.

Fig. 8. Depth profile of refractive index for the ITO film of sample S1 at a wavelength of 474 nm.

Fig. 9. The refractive index and the extinction coefficient versus wavelength for the bottom ITO layer for sample S1 using evaluation of SE data based on the Jung model.

Fig. 10. The refractive index and the extinction coefficient vs. wavelength for the top ITO layer for sample S1 using evaluation of SE data based on the Jung model.

Fig. 11. The measured and generated psi ( $\Psi$ ) values for sample S1 in the wavelength range of 230 - 1690 nm based on the Jung model.

Fig. 12. The measured and generated delta ( $\Delta$ ) values for sample S1 in the wavelength range of 230- 1690 nm based on the Jung model.

Fig. 13. The refractive index and the extinction coefficient versus wavelength for the bottom ITO layer for sample S1 using evaluation of SE data in the wavelength range of 230 – 1690 nm based on the Jung model.

Fig. 14. The refractive index and the extinction coefficient versus wavelength for the top ITO layer for sample S1 using evaluation of SE data in the wavelength range of 230 – 1690 nm based on the Jung model.

### **Table Captions:**

Table I. The thickness values obtained by evaluation of data measured by Filmetrics F20 along with thickness and MSE values obtained by evaluation of data measured by Spectroscopic Ellipsometry (Different models).

Table IA. The sublayer thicknesses calculated in Model 4 and Model 5 for the six samples.

Table II. The thickness values obtained by evaluation of data measured by Filmetrics F20 along with thickness and MSE values obtained by evaluation of data measured by Spectroscopic Ellipsometry. For the evaluation of SE data two different optical models were constructed. The so called Jung model is a three-layer optical model. In the case of Jung model (surface roughness layer plus ITO-upper and ITO- bottom layer) or multilayer model (surface roughness layer plus ITO layer with porosity grading) the „Total thickness” is the sum of the thickness of the ITO

layers and the half of the thickness of the surface roughness layer. The void fraction of the sub-layer adjacent to the surface roughness layer is given for the model with porosity grading.

Table I.

<b>Sample number</b>		<b>S1</b>	<b>S2</b>	<b>S3</b>	<b>S4</b>	<b>S5</b>	<b>S6</b>
<b>FilmetricsF20</b> (eval.:400-800nm) Cauchy dispersion relation	<b>Thickness [nm]</b>	<b>165±5</b>	<b>380±5</b>	<b>545±5</b>	<b>732±5</b>	<b>950±5</b>	<b>1175±5</b>
<b>SE, model 1</b> (eval.:400-800nm) Cauchydispersion relation	<b>Thickness [nm]</b>	<b>141.9±0.4</b>	<b>397±1</b>	<b>412.3±0.8</b>	<b>721±2</b>	<b>944±4</b>	<b>964±4</b>
	MSE	145.7	185.4	97.1	122.9	227.4	142.4
<b>SE, model 2</b> (eval.:400-800nm) surface roughness, Cauchydispersion relation	<b>Thickness [nm]</b>	<b>159.5±0.1</b>	<b>396.9±0.3</b>	<b>416.7±0.3</b>	<b>719.5±0.3</b>	<b>924.0±0.8</b>	<b>953.0±0.3</b>
	MSE	16.2	32	18.3	21.4	41	15.3
<b>SE, model 3</b> (eval.:400-800nm) surface roughness, Drude + Lorentz	<b>Thickness [nm]</b>	<b>158.9±0.2</b>	<b>397.2±0.3</b>	<b>416.2±0.2</b>	<b>715.5±0.3</b>	<b>915.4±0.5</b>	<b>946.8±0.5</b>
	MSE	17.5	36	14.1	18	22.6	20.4
<b>SE, model 4</b> (eval.:400-800nm) surface roughness, Drude + Lorentz + porosity grading	<b>Thickness [nm]</b>	<b>154.8±0.3</b>	<b>393.4±0.3</b>	<b>409.9±0.3</b>	<b>706.5±0.5</b>	<b>909.2±0.3</b>	<b>942.8±0.5</b>
	Void fraction [%]	6.9±0.5	7.5±0.1	4.9±0.2	4.2±0.2	5.06±0.09	2.7±0.1
	n(474nm)	2.18	2.14	2.20	2.19	2.14	2.18
	MSE	15.6	11.2	12.5	16.6	11.1	17.9
<b>SE, model 5</b> (eval.:400- 1690nm) surface roughness, Drude + Lorentz + porosity grading	<b>Thickness [nm]</b>	<b>157.2±0.2</b>	<b>394.5±0.6</b>	<b>409.8±0.4</b>	<b>704.8±0.3</b>	<b>908.2±0.4</b>	<b>927±1</b>
	Void fraction [%]	3.1±0.1	9.8±0.3	4.2±0.2	4.3±0.1	5.8±0.1	6.9±0.3
	n(474nm)	2.13	2.15	2.20	2.20	2.15	2.24
	MSE	11.5	71.6	25.9	19.1	18.6	27.9

Table IA.

Sample number	Sublayer thickness (nm)	
	Model 4	Model 5
S1	1.48	1.49
S2	3.90	3.92
S3	4.11	4.11
S4	7.10	7.08
S5	9.09	9.08
S6	9.47	9.31

Table II.

<b>Sample number</b>		<b>S1</b>	<b>S2</b>	<b>S3</b>	<b>S4</b>	<b>S5</b>	<b>S6</b>
<b>FilmetricsF20,</b> (eval.:400-800nm) (Cauchy dispersion relation)	<b>Thickness[nm]</b>	<b>165±5</b>	<b>380±5</b>	<b>545±5</b>	<b>732±5</b>	<b>950±5</b>	<b>1175±5</b>
<b>SE,</b> <b>Jung model</b> (eval.:300- 1000nm) Three-layer optical model, Drude + Lorentz	Surface roughness thickness [nm]	18.4±0.3	11.50±0.07	5.61±0.06	6.90±0.05	17.57±0.04	9.97±0.08
	Upper-ITO [nm]	104.8±0.7	349.2±0.4	352.4±0.4	657.8±0.6	860.4±0.6	869.2±0.8
	Bottom-ITO [nm]	20±1	30.9±0.5	47.2±0.8	36.5±0.7	35.6±0.7	52.8±0.8
	<b>Total thickness [nm]</b>	<b>134±2</b>	<b>385.6±0.9</b>	<b>402±1</b>	<b>698±1</b>	<b>905±1</b>	<b>927±2</b>
	MSE	12.5	20.7	16.8	19.8	15.7	37.3
<b>SE,</b> <b>Multi layer model</b> (eval.:300-1000nm) Surface roughness, Drude + Lorentz + porosity grading	Surface roughness thickness [nm]	19.03±0.08	14.11±0.07	6.1±0.1	8.59±0.07	18.90±0.06	11.39±0.06
	ITO [nm]	144.1±0.1	381.6±0.3	398.8±0.8	684±2	883±1	911±2
	<b>Total thickness [nm]</b>	<b>153.6±0.2</b>	<b>388.7±0.3</b>	<b>401.9±0.9</b>	<b>688±2</b>	<b>893±1</b>	<b>917±2</b>
	MSE	28.8	45.6	48.3	55.1	37.3	46.7
	Voidfraction [%]	5.8±0.2	12.3±0.2	11.8±0.5	13.2±0.5	12.2±0.3	12.2±0.5

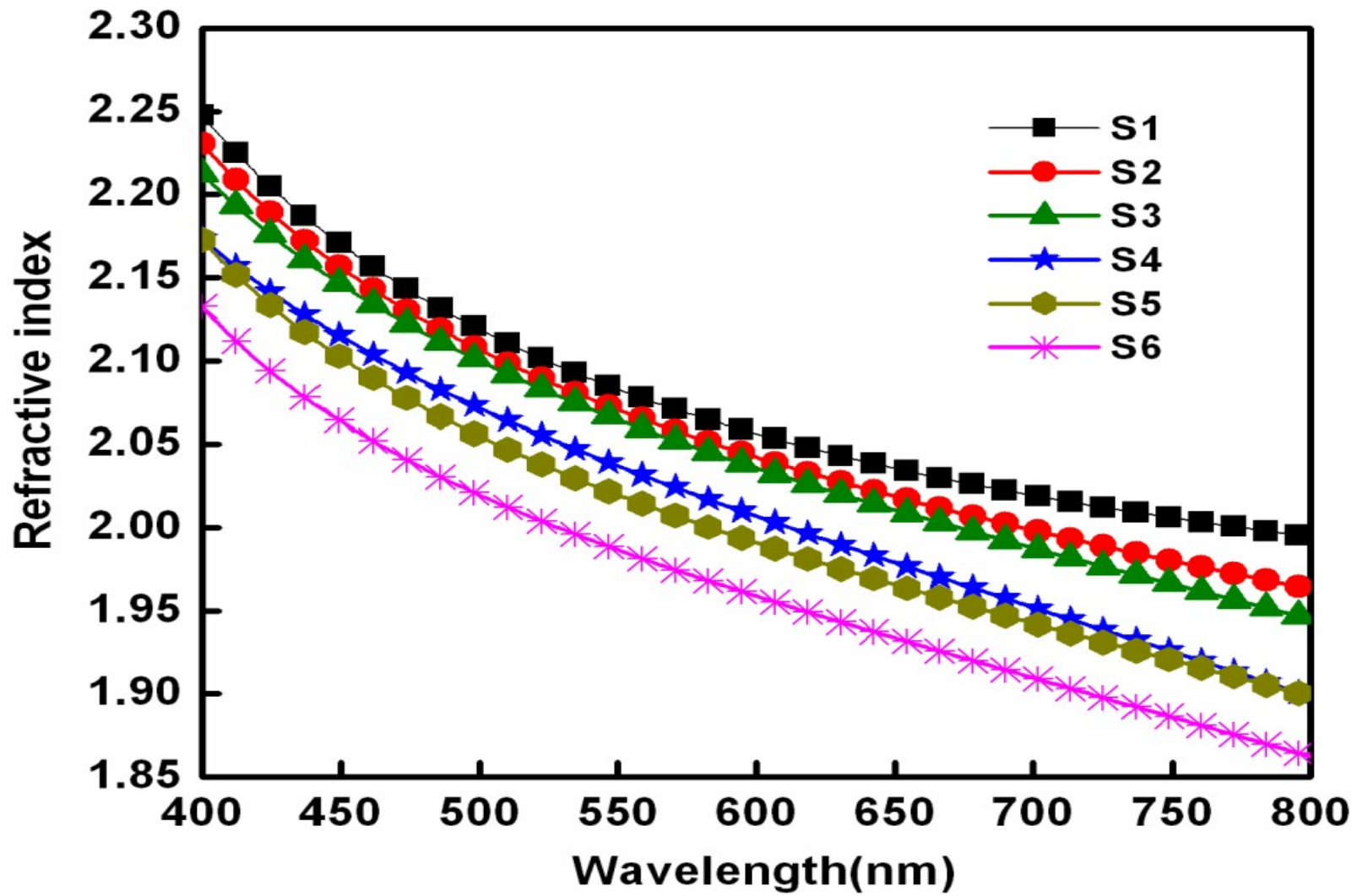


Figure 1.

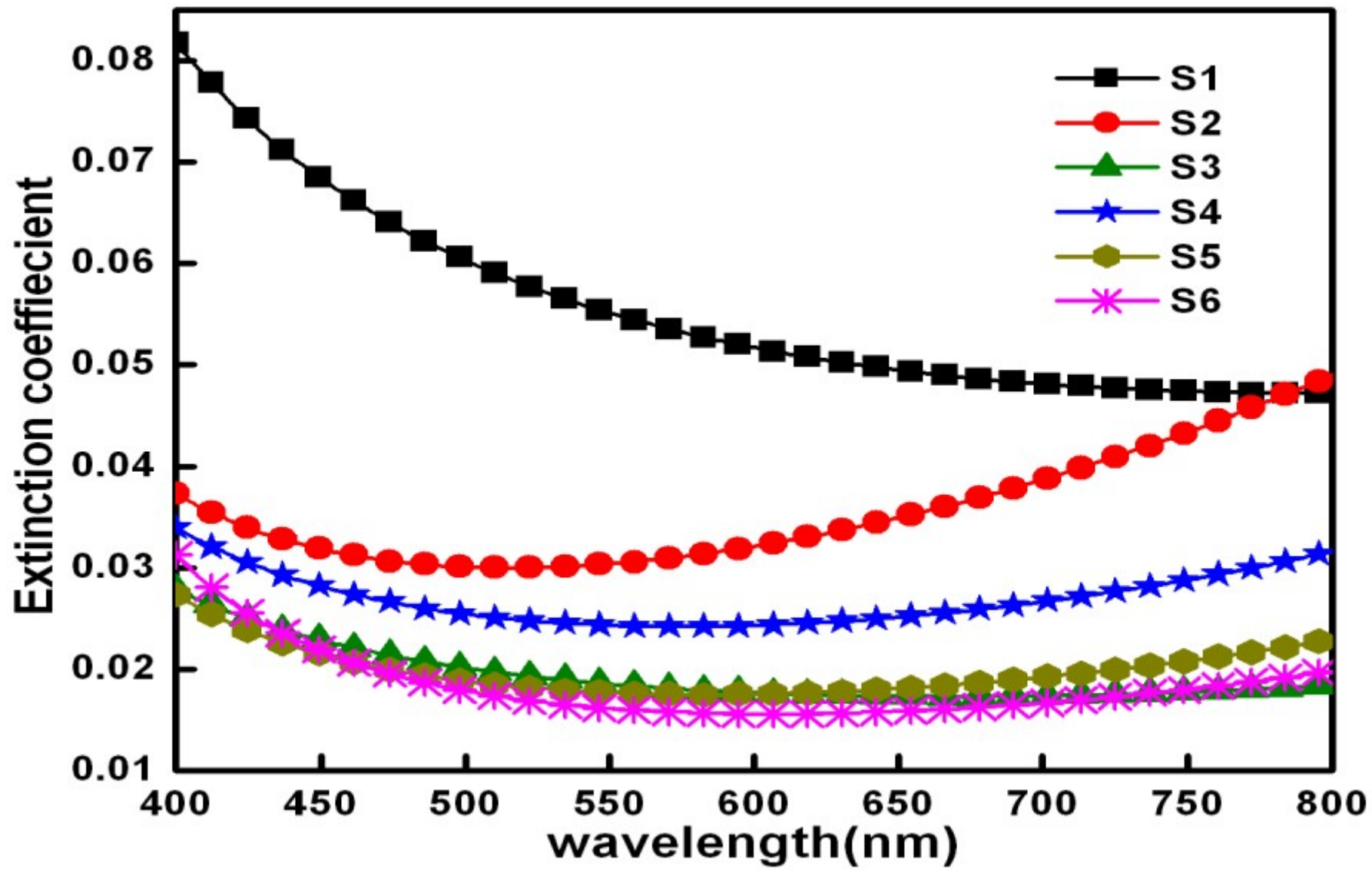


Figure 2.

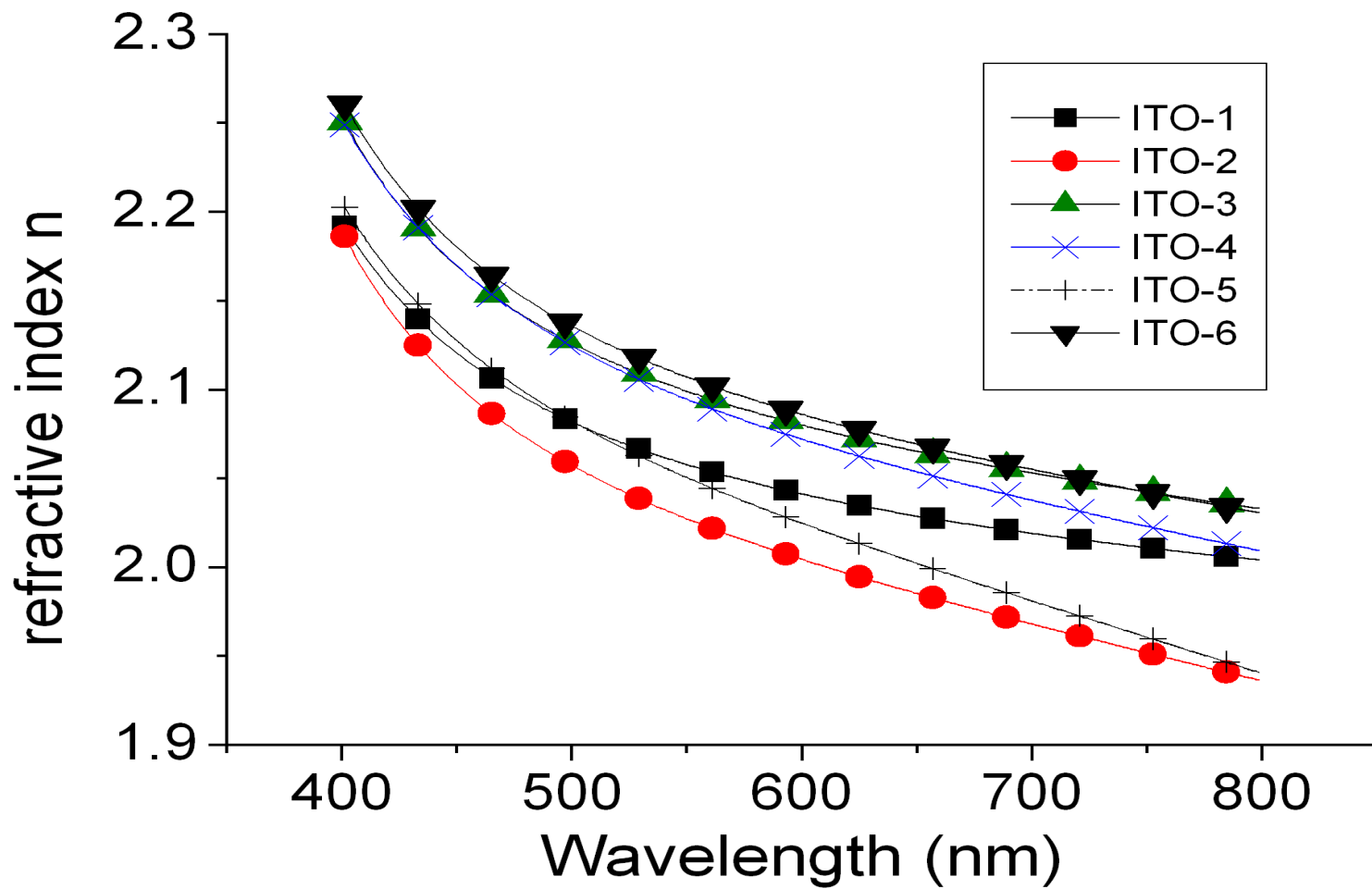


Figure 3.

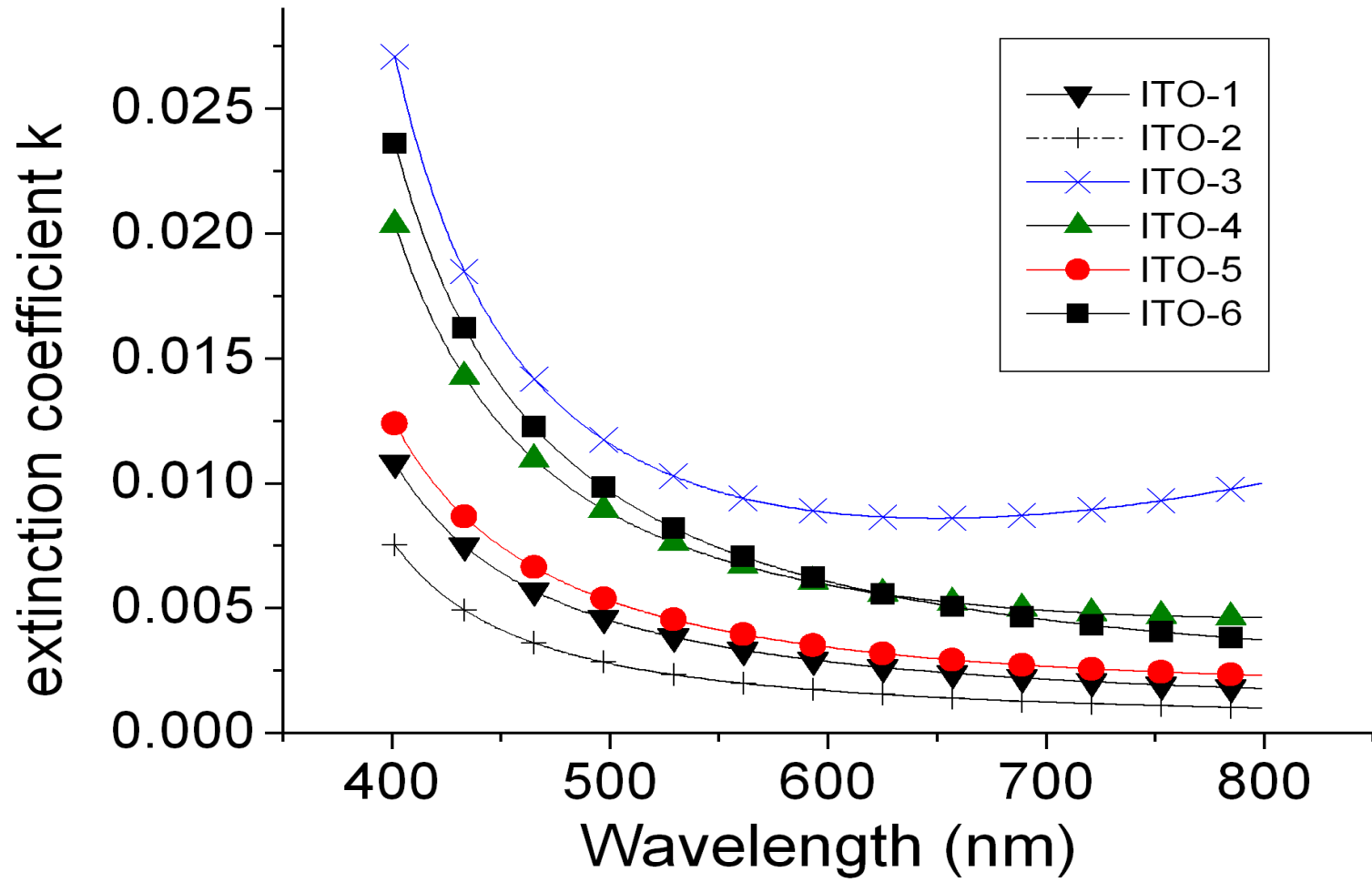


Figure 4.

# Generated and Experimental

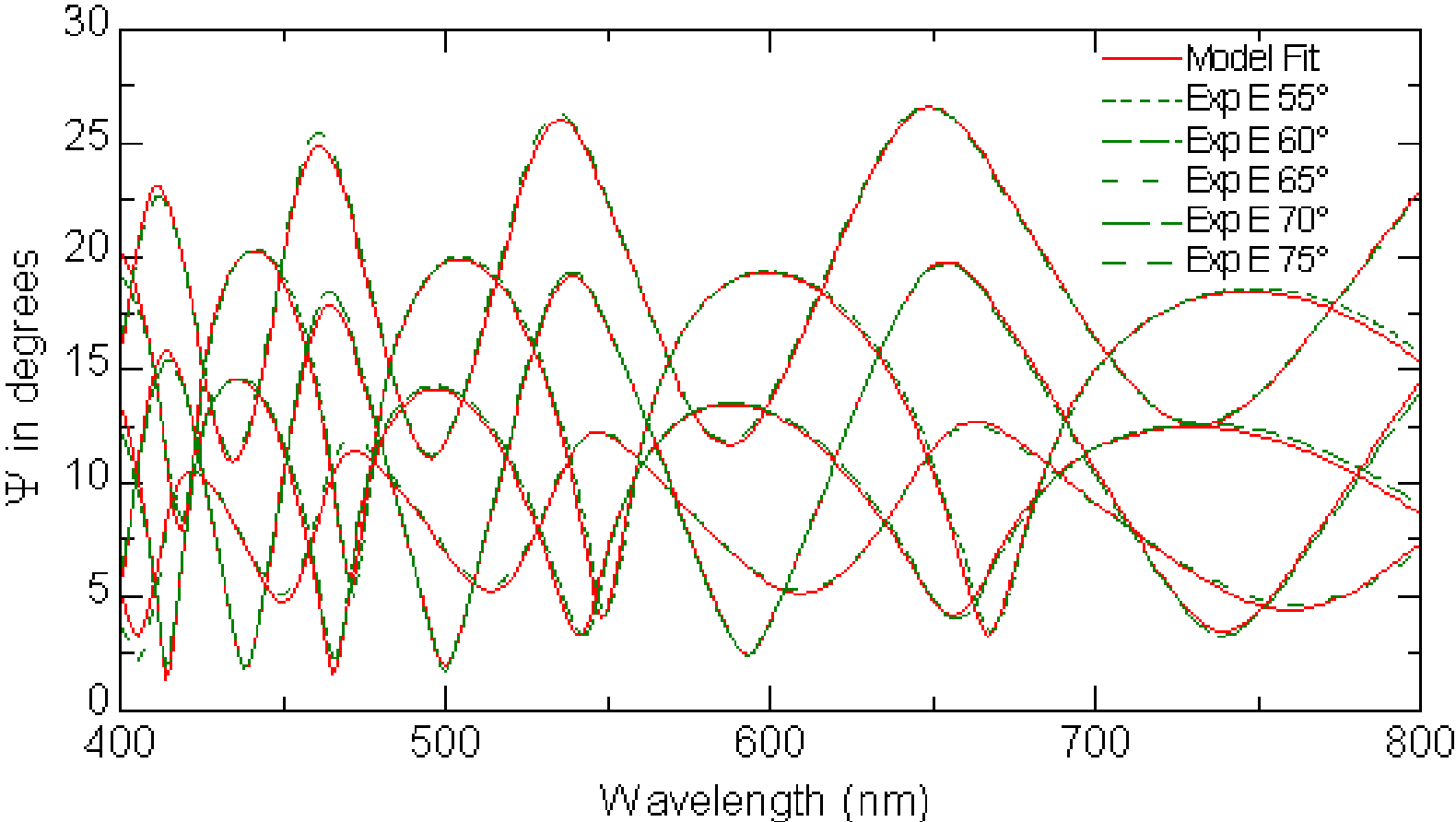


Figure 5.

## Generated and Experimental

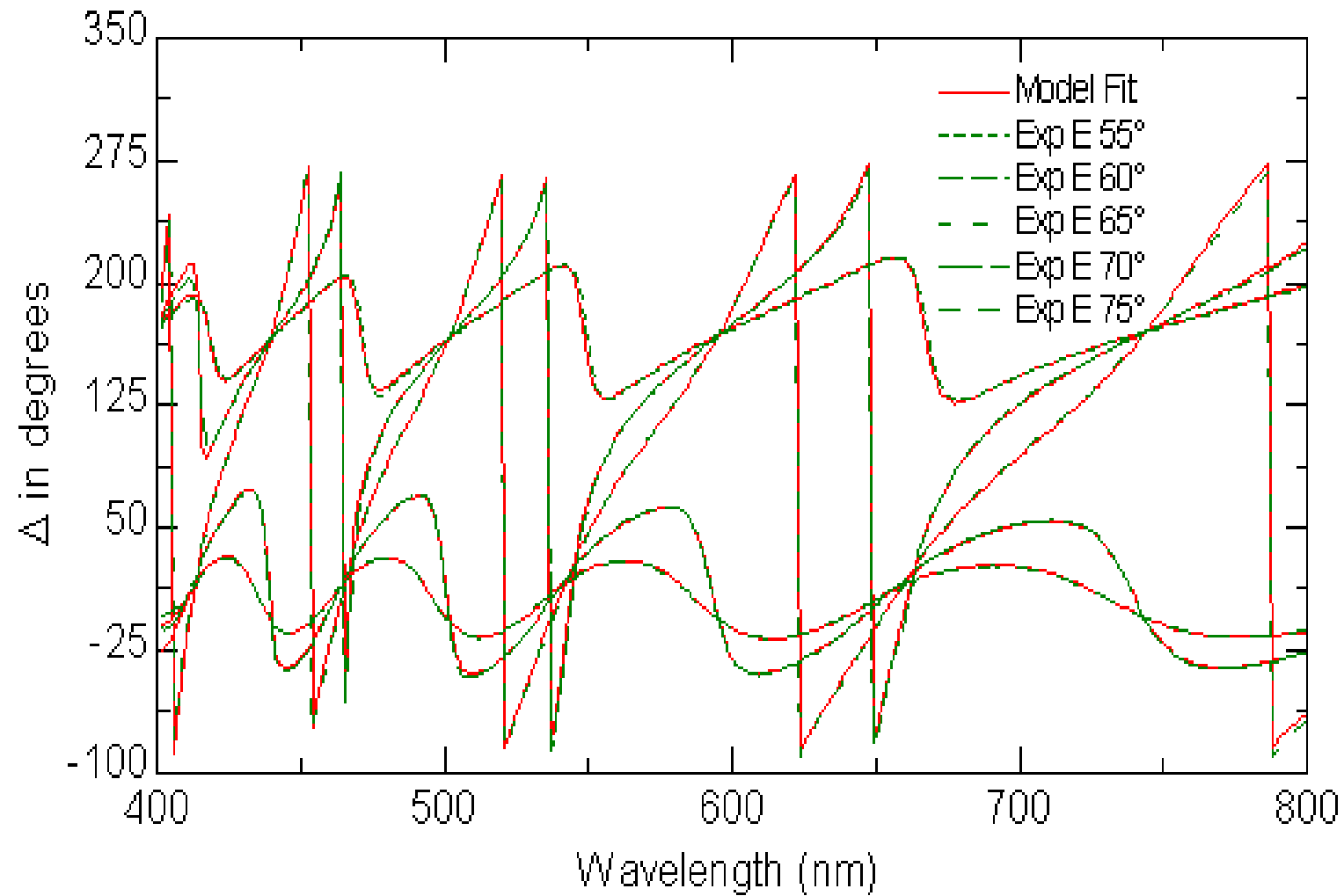


Figure 6.

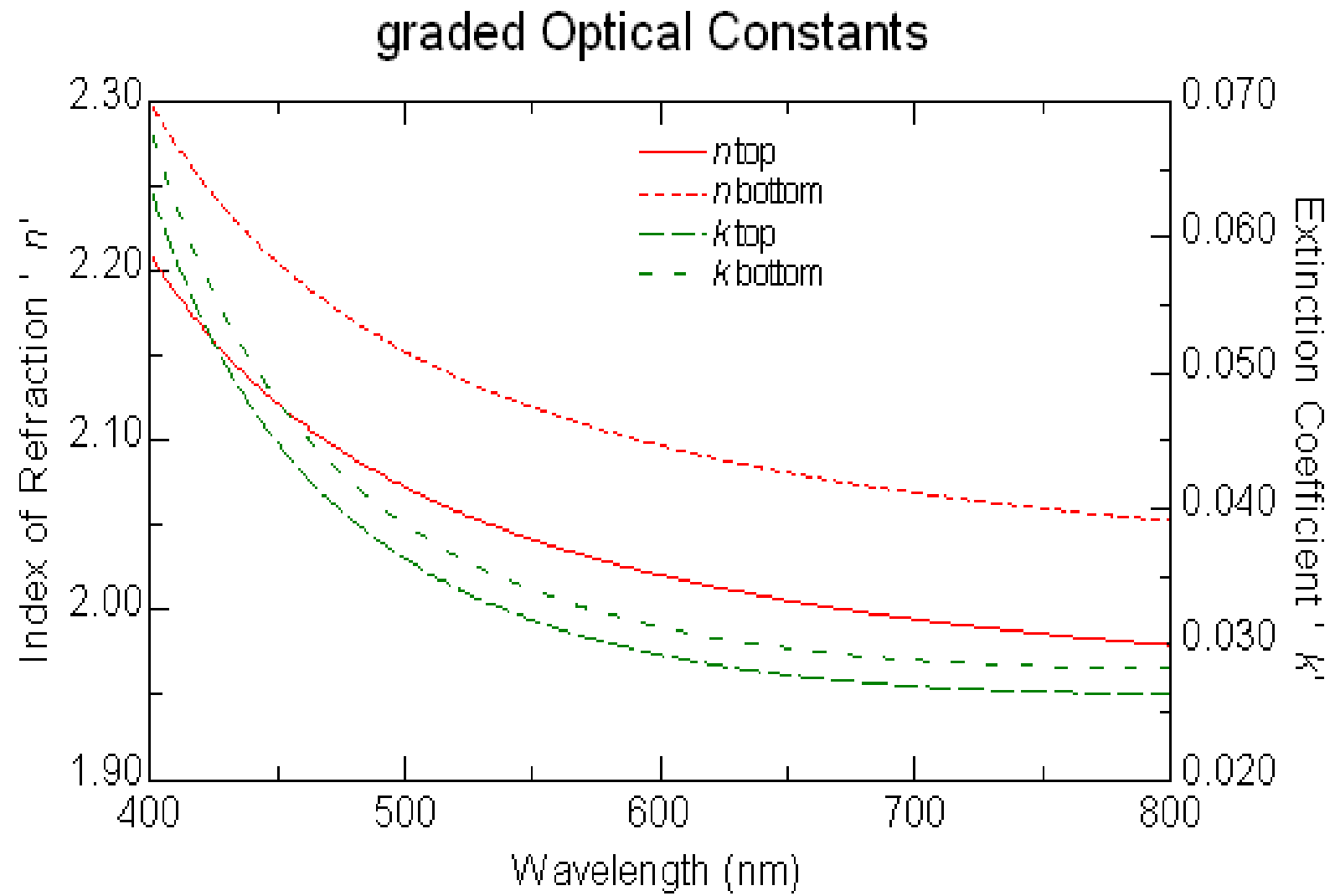


Figure 7.

### Depth Profile of Optical Constants at 474nm

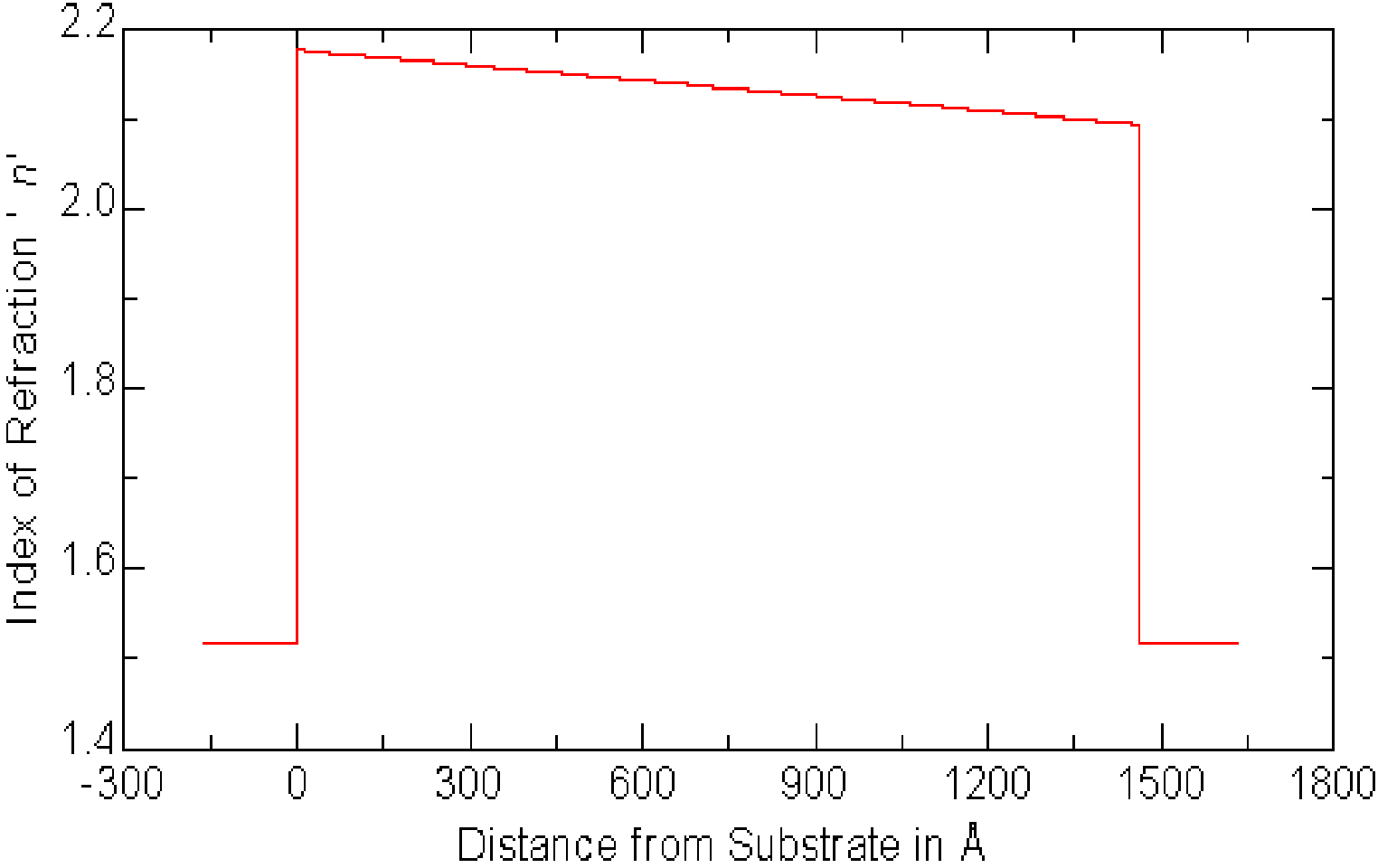


Figure 8.

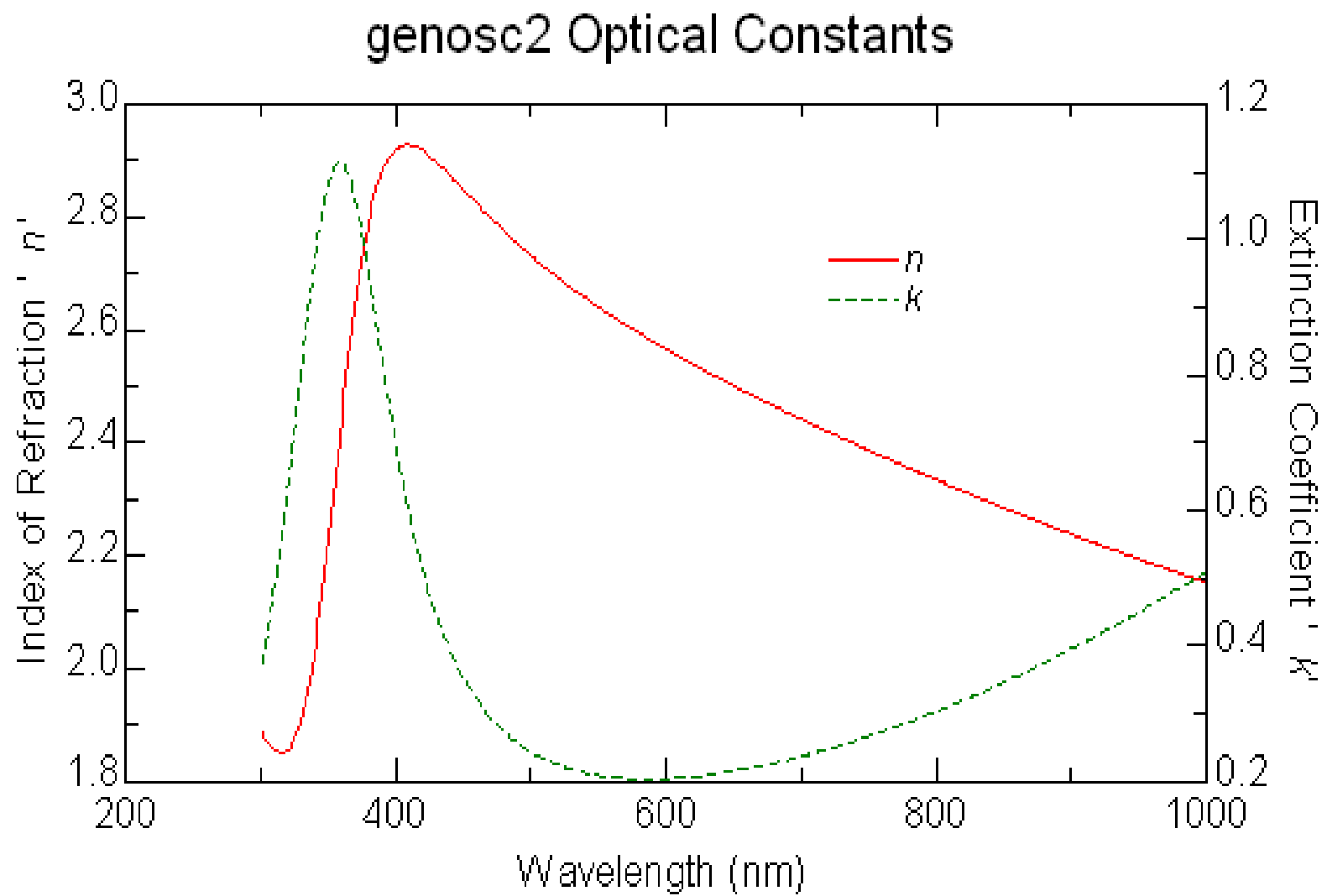


Figure 9.

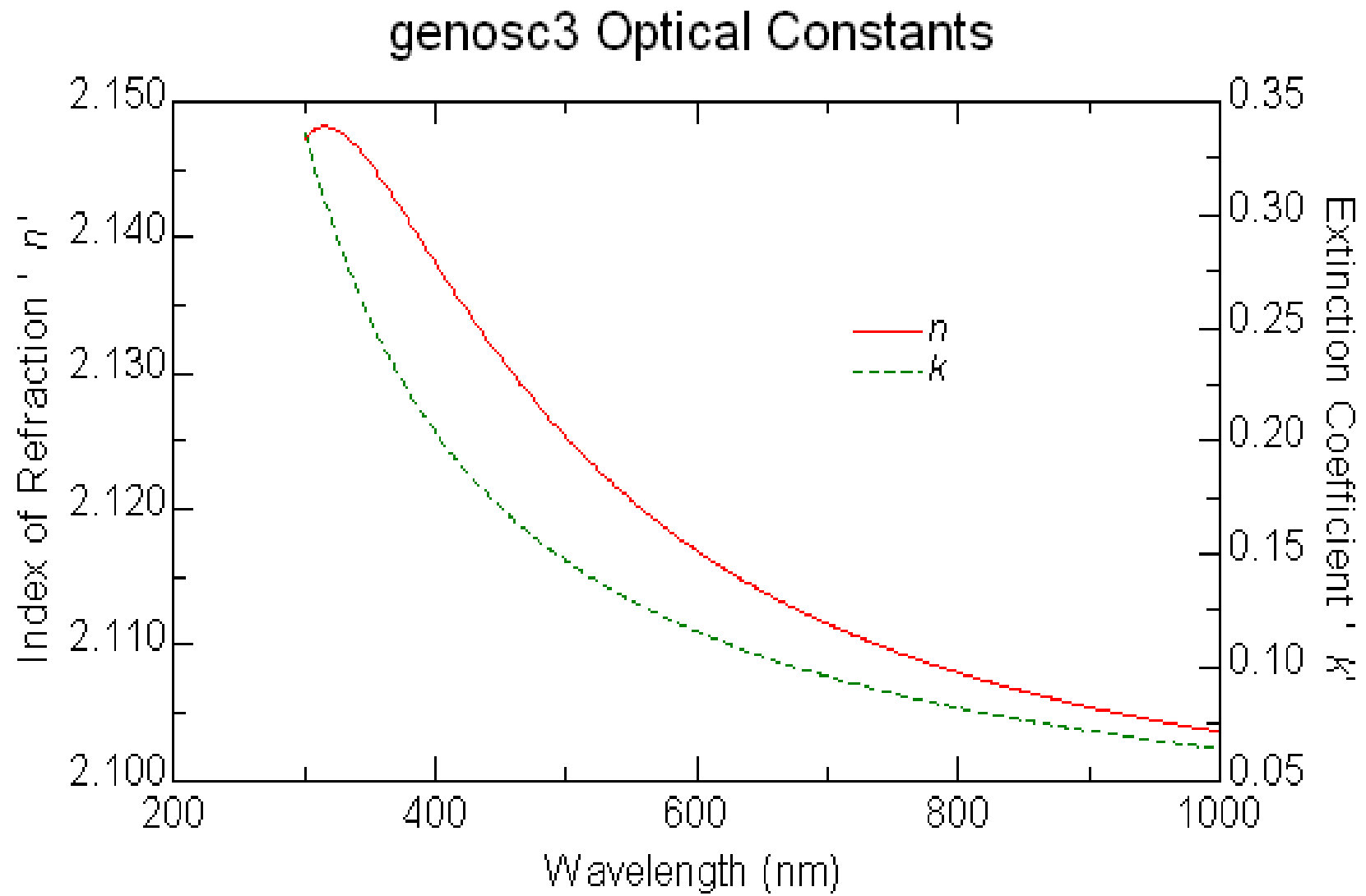


Figure 10.

# Generated and Experimental

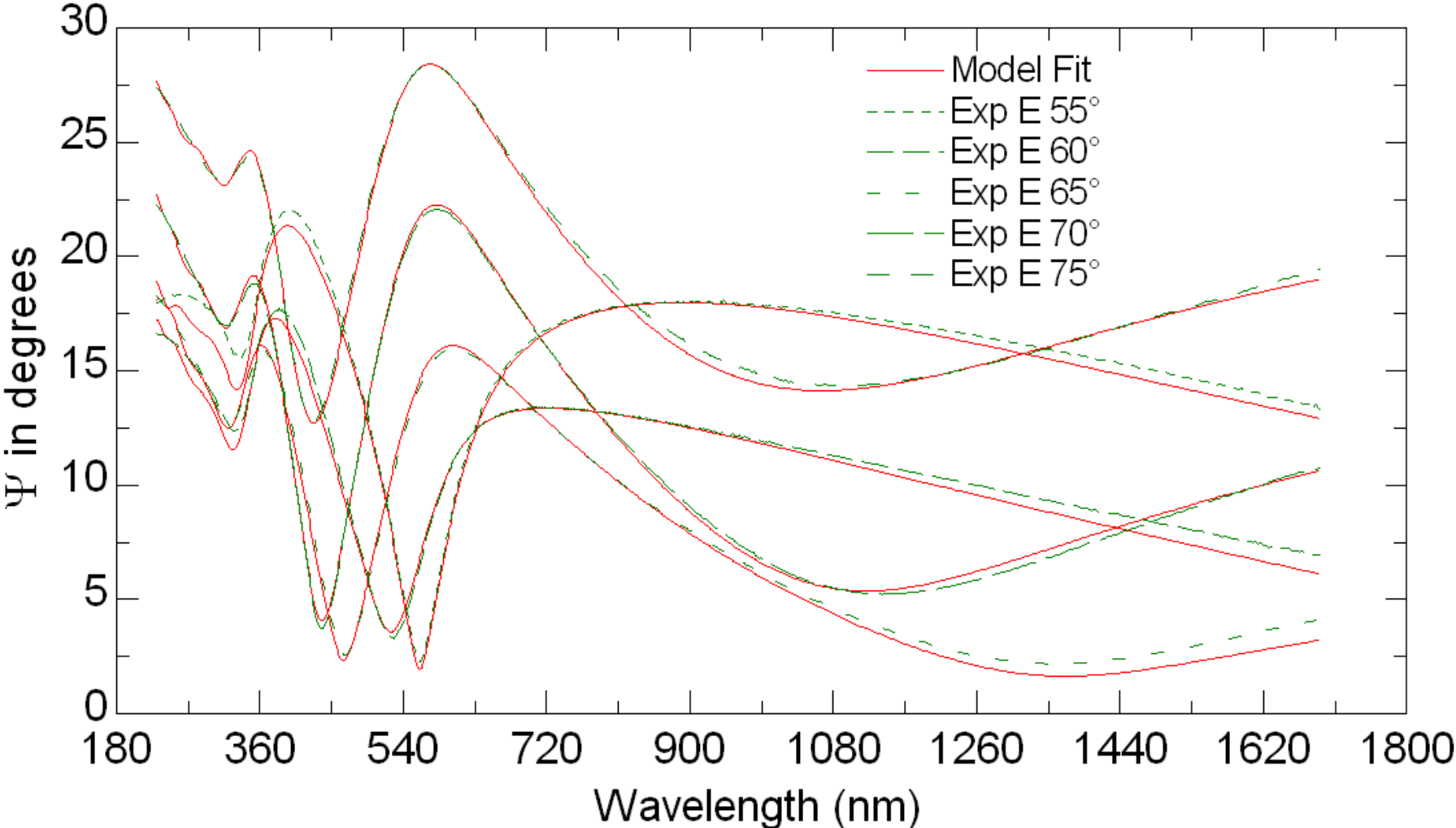


Figure 11.

# Generated and Experimental

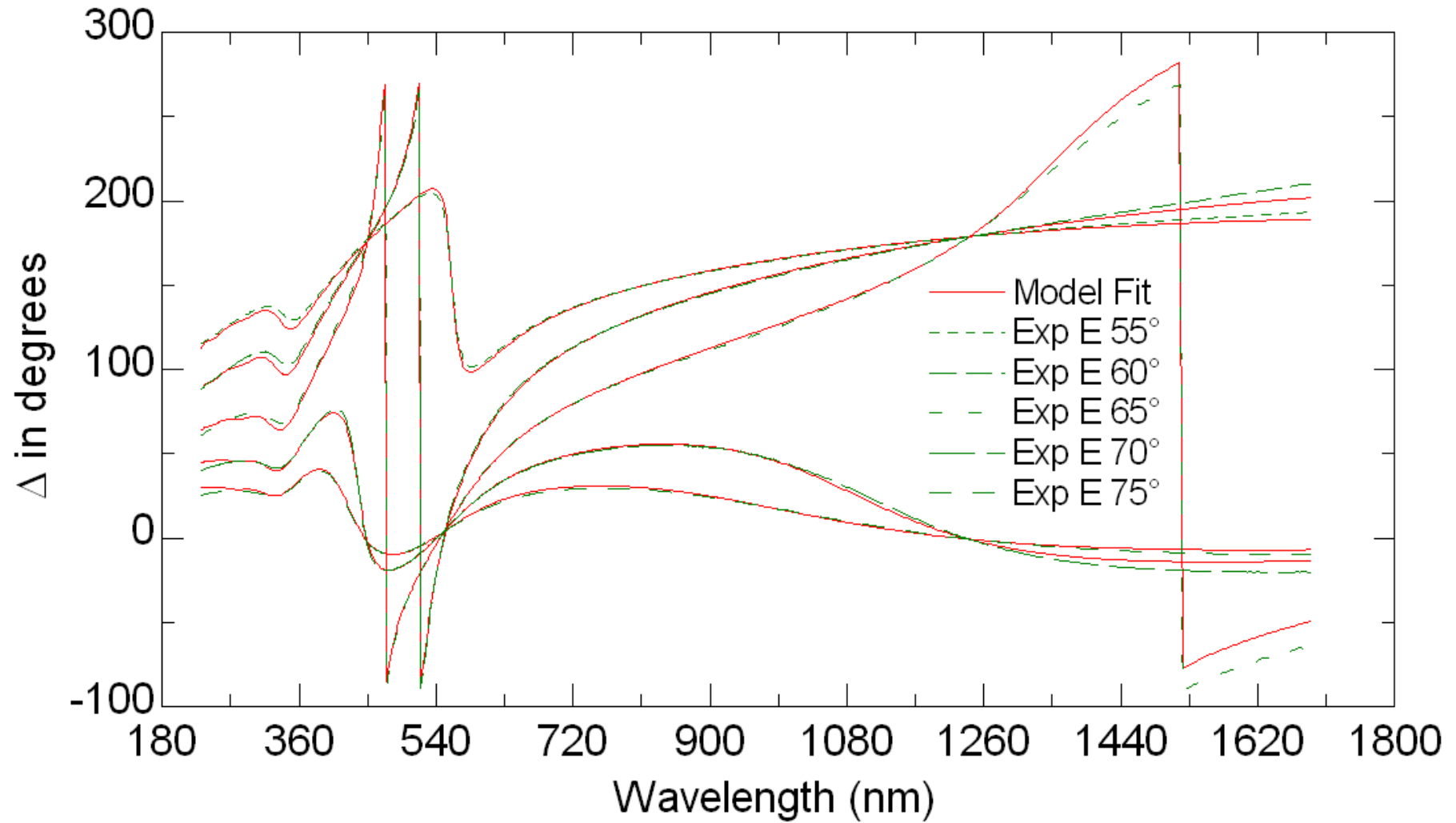


Figure 12.

# genosc2 Optical Constants

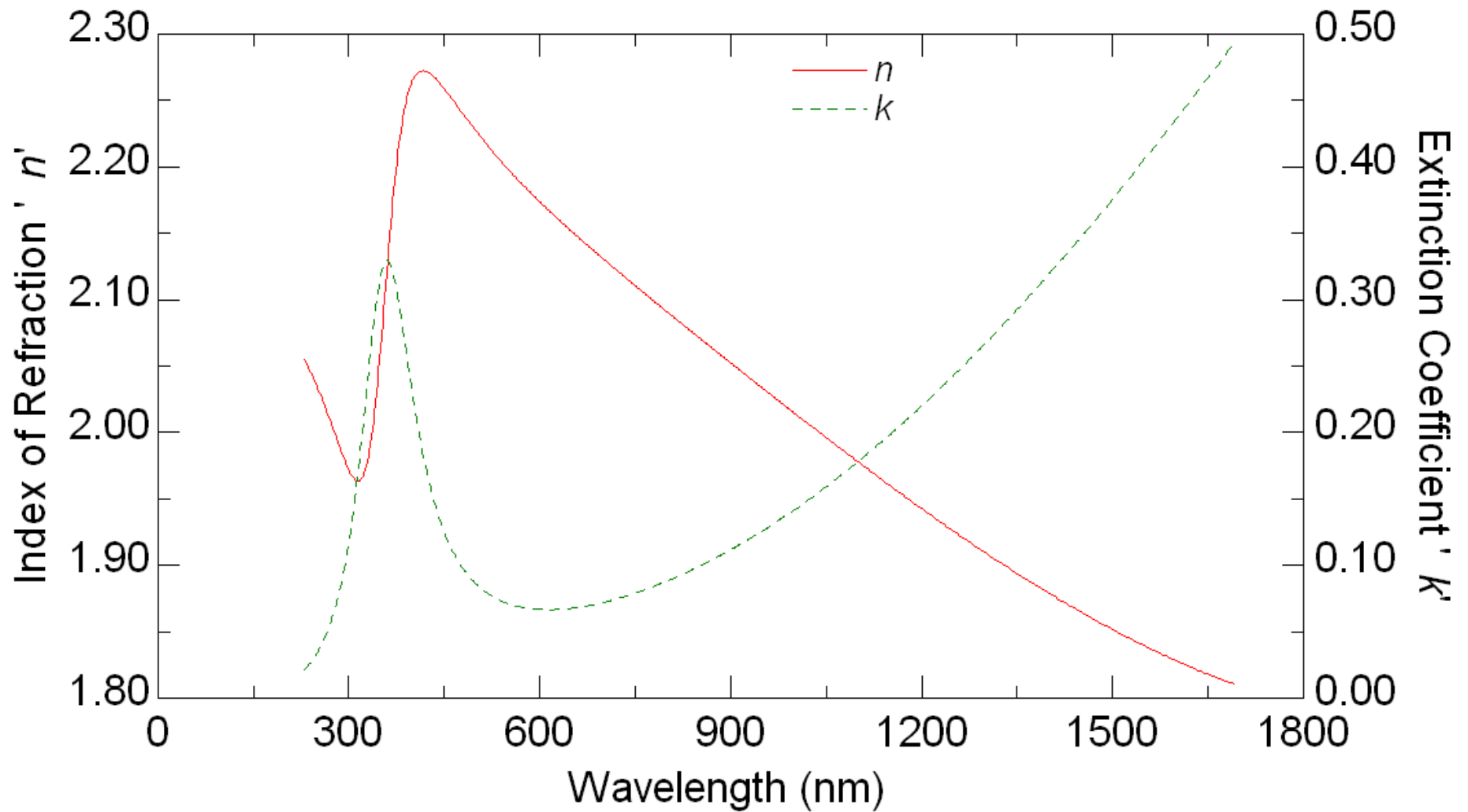


Figure 13.

# genosc3 Optical Constants

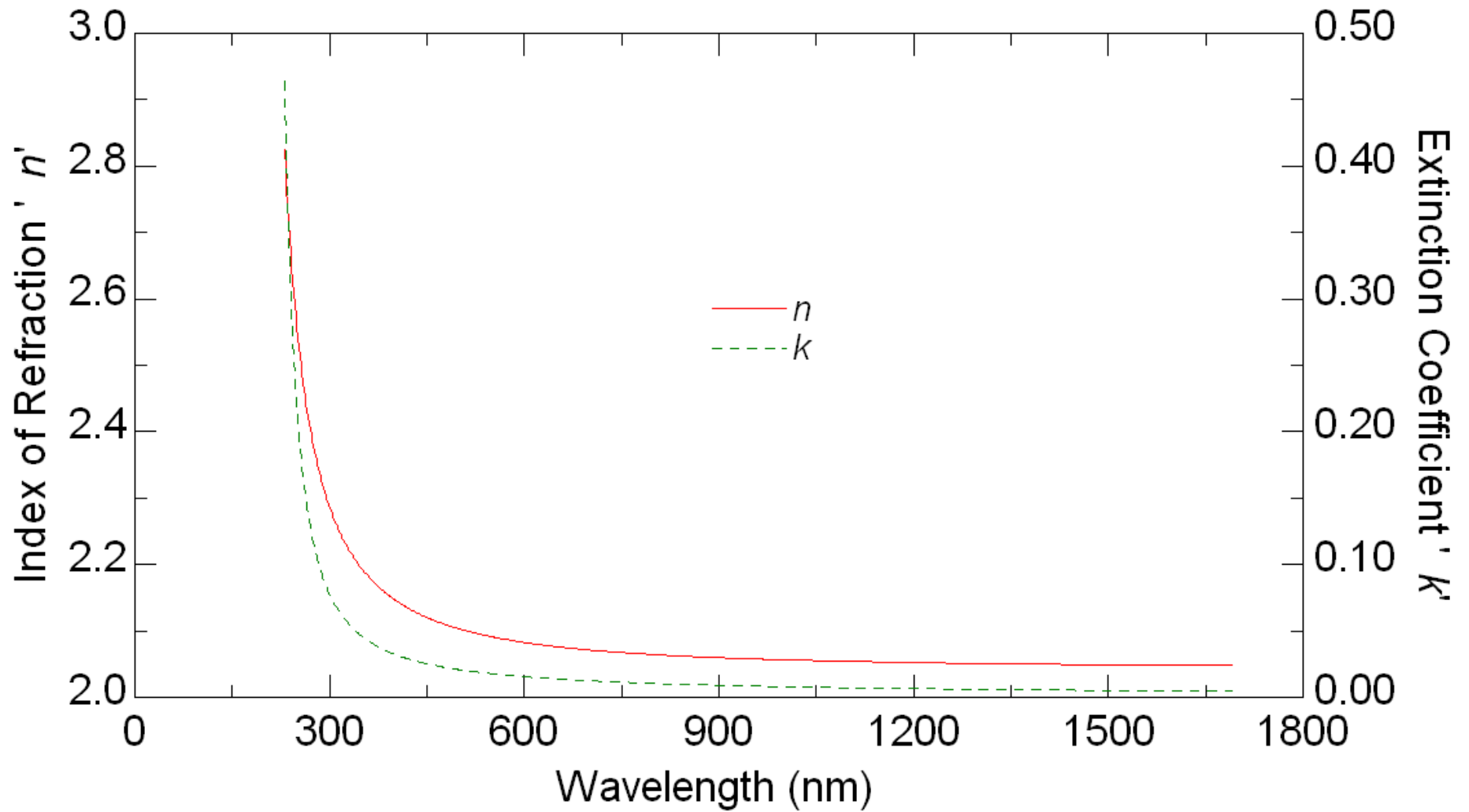


Figure 14.